

1 **Non-destructive assessment of the internal quality of intact persimmon**  
2 **using colour and VIS/NIR hyperspectral imaging**

3 **Sandra Munera<sup>1(\*)</sup>, Cristina Besada<sup>2(\*)</sup>, Nuria Aleixos<sup>3</sup>, Pau Talens<sup>4</sup>, Alejandra**  
4 **Salvador<sup>2</sup>, Da-Wen Sun<sup>5</sup>, Sergio Cubero<sup>1</sup>, José Blasco<sup>1(\*\*)</sup>**

5 <sup>1</sup>Centro de Agroingeniería. Instituto Valenciano de Investigaciones Agrarias (IVIA). Ctra. Moncada-  
6 Náquera Km 4.5, 46113, Moncada, Valencia (Spain) email: blasco\_josiva@gva.es

7 <sup>2</sup>Centro de Tecnología Postcosecha. Instituto Valenciano de Investigaciones Agrarias (IVIA). Ctra.  
8 Moncada-Náquera Km 4.5, 46113, Moncada, Valencia (Spain)

9 <sup>3</sup>Departamento de Ingeniería Gráfica. Universitat Politècnica de València. Camino de Vera, s/n, 46022  
10 Valencia (Spain)

11 <sup>4</sup>Departamento de Tecnología de Alimentos. Universitat Politècnica de València. Camino de Vera, s/n,  
12 46022 Valencia (Spain)

13 <sup>5</sup>School of Food Science and Engineering, South China University of Technology, Guangzhou, 510641,  
14 P. R. China

15  
16 \* These author contributed equally  
17

18 **Abstract**

19 The internal quality of intact persimmon cv. ‘Rojo Brillante’ was assessed through  
20 visible and near infrared hyperspectral imaging. Fruits at three stages of commercial  
21 maturity were exposed to different treatments with CO<sub>2</sub> to obtain fruit with different  
22 ripeness and level of astringency (soluble tannin content). Spectral and spatial  
23 information were used for building classification models to predict ripeness and  
24 astringency through multivariate analysis techniques like linear and quadratic  
25 discriminant analysis (LDA and QDA) and support vector machine (SVM).  
26 Additionally, flesh firmness was predicted by partial least square regression (PLSR).  
27 The full spectrum was used to determine the internal properties and later principal  
28 component analysis (PCA) was used to select optimal wavelengths (580, 680 and 1050  
29 nm). The correct classification was above 92% for the three classifiers in the case of  
30 ripeness and 95% for QDA in the case of astringency. A value of  $R^2 = 0.80$  and a ratio  
31 of prediction deviation (RPD) of 1.86 were obtained with the selected wavelengths for  
32 the prediction of firmness which demonstrated the potential of hyperspectral imaging as

33 a non-destructive tool in the assessment of the firmness, ripeness state and astringency  
34 level of 'Rojo Brillante' persimmon.

35 **Keywords:** *Diospyros kaki*, internal fruit quality, soluble tannins, astringency,  
36 classification, computer vision.

37

## 38 **1. Introduction**

39 Spain is one of the major producers of persimmon (*Diospyros kaki* L.) among European  
40 countries (Plaza et al., 2012). The principal variety grown in Spain is 'Rojo Brillante',  
41 mostly located in the region of Ribera del Xuquer Valley near Valencia (Spain) with  
42 more than 100.000 T per year. This cultivar is very appreciated by consumers because  
43 its good aspect, high size, flavour and absence of seeds. However, this cultivar is  
44 astringent at harvest and the fruit cannot be consumed until a high degree of  
45 overripeness when allowed to rest and soften for a long period after harvest.

46 This has been traditionally a handicap for the commercialization of this fruit since once  
47 the fruit loses the astringency by overripe, it acquires a soft jelly-like consistency being  
48 difficult to handle and eat. Now, some methods have been developed to eliminate  
49 quickly the astringency without losing the firmness, as exposing fruit to high CO<sub>2</sub>  
50 concentrations (95-100%) during 18 to 24 hours. This method is based on promoting  
51 anaerobic respiration in the fruit, giving rise to an accumulation of acetaldehyde which  
52 reacts with the soluble tannins that are the responsible for the astringency (Matsuo et al.,  
53 1991). In figure 1 can be appreciated the differences between a persimmon naturally  
54 deastringed by overripeness and another deastringed using a CO<sub>2</sub> treatment. Since the  
55 success of the treatment was demonstrated (Salvador et al., 2007; Besada et al., 2010), it  
56 has been adopted by industry as the standard deastringency method, and utilized to give  
57 the fruit in addition a sweet taste and firm texture similar to the apple, highly

58 appreciated by the consumers. However, the effectiveness depends on the fruit firmness  
59 at harvest, since maturation process is accompanied by a gradual decrease of firmness  
60 (Salvador et al., 2008). A problem is that the stage of maturity at harvest is currently  
61 determined based on the visual inspection of experienced growers or using colorimeters  
62 due the relationship between the changes in external colour and the internal changes  
63 (Salvador et al., 2006 & 2007).

64 The current way to know the level of astringency in the fruit after CO<sub>2</sub>-treating is by  
65 destructive measurement of soluble tannin content (ST) in random fruits by means of  
66 the tannin print method (Matsuo and Ito, 1982) which consists of using a FeCl<sub>3</sub>-  
67 impregnated filter paper to obtain a print of the content and distribution of the tannins  
68 trough the reaction with the FeCl<sub>3</sub> in the paper. Then, this print is visually assessed by  
69 trained workers being this method subjective and destructive and therefore the  
70 development of other new non-destructive and accurate methods is needed.

71 Computer vision systems have been traditionally used to create tools for the objective  
72 estimation of the quality of intact fruit production (Cubero et al., 2011) and have  
73 already been explored to assess quality of persimmon. Mohammadi et al., (2015) used  
74 colour information to determine the maturity of this fruit through colour analysis and  
75 classify the fruit into three commercial maturity stages.

76 Standard computer vision systems tend to mimic the human eye and hence are based on  
77 sensors sensible to visible wavelengths. But to analyse internal composition it is  
78 necessary the use of technology sensible to non-visible wavelengths related with  
79 chemical compounds. This can be achieved by using hyperspectral imaging (Lorente et  
80 al., 2012) that is a powerful non-invasive technology that allows obtaining the spatial  
81 distribution of the spectral information and it is being used from recent in the internal  
82 quality inspection of food (Cheng et al., 2016a; Cheng et al., 2016b, Gómez-Sanchis et

83 al., 2013) or to assess some properties of fruits like the ripeness in apples (ElMasry et  
84 al., 2008), citrus fruits (Folch-Fortuny et al., 2016), pepper (Schmilovitch et al., 2014),  
85 or mango (Velez-Rivera et al., 2012).

86 Hyperspectral imaging in persimmon has been used by Munera et al., (2017) to create  
87 images showing the distribution of the predicted astringency of each pixel in the fruit,  
88 and by Wei et al., (2014) to predict firmness. However, in this work, the authors  
89 claimed that more research is needed to include more samples as well as different  
90 regions and different postharvest treatments to ascertain the discrimination power of this  
91 method and it is therefore necessary to investigate new methods especially to  
92 discriminate among fruits with slightly different stages of maturity or levels of  
93 astringency as those exposed to a CO<sub>2</sub> treatment, to achieve a demand from both the  
94 industry and the consumers. This work proposes a new non-destructive approach based  
95 on visible and near infrared (VIS/NIR) hyperspectral imaging and multivariate analysis  
96 to determine the firmness, ripeness state and astringency level of intact persimmon  
97 ‘Rojo Brillante’ as alternative to the current destructive and/or subjective techniques.

## 98 **2. Materials and methods**

### 99 **2.1 Plant material and internal quality assessments**

100 A total of 90 persimmon (*Diospyros kaki* cv. ‘Rojo Brillante’) fruits were harvested in  
101 L’Alcudia (Valencia, Spain) at three different stages of commercial maturity (M1, M2  
102 and M3) corresponding to different moments of the season (early November, end  
103 November, and mid December). A total of 30 fruits, with apparently similar size and  
104 colour were collected for each maturity stage. In order to obtain three different levels of  
105 astringency, the fruits in each maturity stage were equally divided into three sets. The  
106 first set (control fruits with high astringency, HA) consisted of fruits not treated, the  
107 second set (medium astringency fruits, MA) consisted of fruits treated in closed

108 containers at 20 °C with 90% of relative humidity (RH) and 95% of CO<sub>2</sub> for a period of  
109 12 h, and the remaining set (non astringent fruits, NA) were fruits treated under the  
110 same conditions for 24 h.

111 After each treatment, all the fruits were measured using a colorimeter, a digital camera,  
112 and a hyperspectral imaging system. Later, flesh firmness of all fruits was determined  
113 by means of a universal testing machine (4301, Instron Engineering Corp., MA, USA)  
114 equipped with an 8 mm puncture probe. The crosshead speed during the firmness  
115 testing was 10 mm/min. During the test, the force increased smoothly until it drastically  
116 decreased when the flesh was broken and the maximum peak force was registered.  
117 Results were expressed as the mean of the load (in N) required for breaking the flesh of  
118 the fruit on the two sides after peel removal. To analyse the astringency of the fruits,  
119 they were sliced and frozen at -20 °C to determine soluble tannins using the Folin-  
120 Denis method (Taira, 1995), as described by Arnal and Del Río (2004). This method is  
121 based on the reduction of the Folin-Ciocalteu reagent by soluble tannins in alkaline  
122 solution. Calibration curve was made with gallic acid. Soluble tannins were extracted by  
123 homogenization of 5 g of flesh with 25 mL of 80% methanol solution. Thereafter,  
124 samples were filtered and centrifuged for 20 minutes and the supernatant was reserved.  
125 More supernatant was extracted from the precipitant with methanol 80% and added to  
126 the first. The supernatant was diluted in water at 1:7 and then Folin-Ciocalteu reagent 1  
127 N was used to conduct the reaction. After 3 minutes 1 ml of saturated Na<sub>2</sub>CO<sub>3</sub> was  
128 added, and the absorbance of the mixture at 725 nm was measured by colorimetry after  
129 stand for 1 h.

## 130 **2.2. Colour analysis**

131 At harvest this fruit presents a uniform colour that ranges from bright to dark orange  
132 depending on the maturity being the colour a good indicative of this property (Salvador

133 et al., 2007). The external colour the fruit under study was characterised using two  
134 techniques. On the one hand, a colorimeter (CR-300, Konica Minolta Inc, Tokyo,  
135 Japan) was used to obtain the colour at three points of the equatorial part of the fruit.  
136 Hunter Lab colour coordinates were obtained by the average of three measures. On the  
137 other hand, the colour was also evaluated through images of the two sides of each fruit.  
138 The image acquisition system consisted on a digital camera (EOS 550D, Canon Inc,  
139 Japan) arranged into a squared inspection chamber that included a calibrated and  
140 uniform illumination system composed of eight fluorescent tubes (BIOLUX 18W/965,  
141 6500 K, Osram GmbH, Germany). The angle between the axis of the lens and the  
142 sources of illumination was approximately 45° to avoid direct reflections to the camera  
143 (Diago et al., 2015), but due to the spherical shape of the samples these reflections  
144 could not be totally avoided this way and hence cross-polarization was also used  
145 (ElMasry et al., 2012).

146 A total of 180 images were obtained with a size of 2592 x 1944 pixels and a resolution  
147 of 0.11 mm/pixel. Figure 2 shows examples of images of the fruits in the three maturity  
148 stages. For each image, the mean red, green and blue (RGB) colour values of the pixels  
149 of the skin were obtained using the application Food\_ColorInspector (free download at  
150 <http://www.cofilab.com>). RGB values were later converted to Hunter Lab colour space  
151 for analysis using the equations described in Mendoza et al., (2006) and HunterLab  
152 (1996) for illuminant D65 and standard observer 10°. The Hunter Lab coordinates were  
153 finally transformed to the colour attributes Hunter luminosity (L), Hunter hue (h) and  
154 Hunter chroma (C) (Hutchings, 1999). In addition, RGB values were transformed into  
155 HSI (hue, saturation, intensity) values and other indices were estimated such as the  
156 ratios  $a/b$  and  $a/L$  and the colour index ( $CI=1000a/Lb$ ) (Salvador et al., 2006).

### 157 **2.3 Hyperspectral imaging**

158 Hyperspectral images of the intact persimmons in the spectral range 450-1020 nm were  
159 acquired using a camera (CoolSNAP ES, Photometrics, USA) coupled to two liquid  
160 crystal tuneable filters (LCTF) (Varispec VIS-07 and NIR-07, Cambridge Research &  
161 Instrumentation, Inc., MA, USA). The illumination system consisted of 12 halogen  
162 lights arranged equally into a domo inspection chamber where whole fruits were  
163 manually introduced (Figure 3).

164 Hyperspectral images with a spatial resolution of 0.14 mm/pixel and a spectral  
165 resolution of 10 nm were captured in both sides of each fruit (Figure 4), which lead to a  
166 tagged database of 180 hyperspectral images. In each image, a region of interest (ROI)  
167 of  $225 \times 225$  pixels in the central part of the fruit was selected and analysed as the  
168 average of spectrum of all pixels for maturity and firmness analysis since these  
169 properties are quite uniformly distributed in the fruit. However, for the case of the  
170 astringency, the individual spectrum of each pixel in the ROI was included in the  
171 models due the uneven distribution in the fruit of tannins responsible of the astringency.  
172 To obtain the relative reflectance of a pixel in the position  $(x,y)$  of the monochromatic  
173 band  $\lambda$ , the original reflectance was corrected using a dark and white reference  
174 (Spectralon 99%, Labsphere, Inc, NH, USA) following the procedure described in Gat  
175 (2000).

## 176 **2.4 Data analysis**

177 Analysis of variance (ANOVA) and Tukey multiple range test (Statgraphics  
178 Centurion XVI - Statpoint Technologies Inc., Virginia, USA) were used to show the  
179 effects of ripeness on colour parameters obtained with both, colorimeter and computer  
180 vision system. In this analysis, the three maturity stages were the observed values ( $Y$ )  
181 and the Hunter Lab colour coordinates captured by both the colorimeter and the vision  
182 systems were the predictive variables.

183 Hyperspectral images consisted of 67 wavelengths and therefore the spectra obtained  
184 from these images were distributed in a matrix with 67 columns each corresponding to  
185 the reflectance value of each band where the rows represented the fruits. In addition, the  
186 pixels were labelled as belonging to any of the maturity stages (M1, M2 and M3) and  
187 treatments (HA, LA, NA) to carry out the analysis for firmness and astringency  
188 prediction. First step was a preprocessing of data using Standard Normal Variate (SNV)  
189 to remove scatter effects from original spectral data (The Unscrambler X 10.1, CAMO  
190 Software, Oslo, Norway). Classification models to sort the fruit by ripeness stage and  
191 treatment duration (astringency level) were developed using linear and quadratic  
192 discriminant analysis (LDA & QDA), and support vector machine (SVM) (Dutta et al.,  
193 2016). The difference between LDA and QDA classifier is that LDA uses pooled  
194 covariance to assign an unknown sample to one of the pre-defined groups while QDA  
195 uses the covariance of each group instead of pooling them (Naes et al., 2002). On the  
196 other hand, the SVM algorithm was developed based on the concept of hyperplane and  
197 support vectors, using a linear function kernel with C value set to 1. In addition,  
198 firmness prediction was conducted by partial least square regression (PLSR) (Cheng et  
199 al., 2015b) using the ratio of prediction deviation (RPD), that was defined by Williams  
200 (1987) as the ratio of standard deviation of reference values in training set to the root  
201 mean square error of prediction (RMSEP).

202 Hyperspectral systems capture a huge amount of information that is redundant and  
203 correlated, especially between contiguous wavelengths (Lorente et al., 2012). Therefore,  
204 principal component analysis (PCA) was used to know if it was possible to obtain good  
205 prediction using a reduced subset of bands. Four different PCA models were built, one  
206 of using the spectral data of the ripeness assessment and the other three PCA with data  
207 of the astringency assessment for each harvest. The variables (wavelengths) were



208 chosen on the basis of the size of coefficients or loadings in the eigenvectors of the  
209 principal components.

### 210 **3. Results and discussion**

#### 211 **3.1. Maturity assessment**

212 Several differences can be observed among the spectra of the fruit in the three maturity  
213 stages shown in Figure 5. Fruits of M1 gave higher reflection values than the others in  
214 the visible region, which is in agreement with the colour analysis. An absorption peak  
215 was found around the bands 670-680 nm only for fruits in M1 stage which could be due  
216 the presence of chlorophyll in the more unripe fruit (Lleó et al., 2011). However, the  
217 fruits in M2 stage are those which gave a higher reflection in the NIR region that can be  
218 due to the chemical differences among fruit at different ripeness. The absorption peak  
219 observed around 900-1050 nm could be assigned to water absorption band. This peak  
220 was higher in M3, which may be related to water content increases in the flesh during  
221 the onset of ripening, which in other fruits has been related to cell breakage and osmotic  
222 movement of water from the flesh to the peel.

223 The PCA model generated with the 67 wavelengths was analysed to identify the  
224 variable with the highest factor loadings since they reflected the importance of each  
225 wavelength in discriminating differences in the fruit (Wang et al., 2012). The loadings  
226 of the first two principal components were used for wavelength selection because these  
227 were responsible for 96% of the variance in the spectral data. The wavelengths  
228 corresponding to higher module values (peaks and valleys) at these particular principal  
229 components were selected as candidates for optimum wavelengths (Rodríguez-Pulido et  
230 al., 2013) (Figure 6). Four optimum wavelengths (450, 580, 680, and 1050 nm) were  
231 thus identified for discrimination purposes of different maturity stages. Wavelengths  
232 450 nm and 680 nm are related with the presence of beta-carotene and chlorophyll a

233 respectively. On the other hand, the importance of the wavelength 580 nm can be due to  
234 the colour changes during ripeness since it corresponds to the yellow colour. This would  
235 be in accordance with the ranges of h and C values shown in Table 3. The band 1050  
236 nm could be related with an absorption region of water content although the peak is  
237 situated below 1000 nm (Lu and Peng, 2006).

238 Statistical models to classify the fruit into maturity stages were developed using the  
239 spectra of the full spectra and only the selected wavelengths. In order to build and  
240 validate the model, a 3-fold cross validation procedure was used (Simon, 2007). The  
241 data set of pixels was randomly partitioned into three disjoining subsets. The classifier  
242 development process was repeated three times using each two different subsets and the  
243 resulting classifiers used to classify the remaining test set. Finally the results of the three  
244 iterations were averaged.

245 The four selected bands were used to build the models but also the possible  
246 combinations of three bands resulting that using only 580 nm, 680 nm, and 1050 nm,  
247 the results were similar to those achieved using the four bands. Using only these three  
248 selected wavelengths the success rate of correct classification was slightly lower (mean  
249 value of 94.8%) than using the full spectrum (mean value of 98.5%) as shown in Table  
250 1.

251 Comparing the three classification methods, all of them achieved a good classification  
252 above 98% using the all wavelengths. Moreover, using only the three selected  
253 wavelengths only LDA showed an important reduction in the success rate while the  
254 other two classifiers still remain above 95% which is considered as a good result for a  
255 non-destructive technique.

### 256 **3.2. Firmness prediction**

257 Table 2 shows the firmness evolution with the harvesting time (ripeness). A model  
258 based on PLSR was built to know if it was possible to predict this property in this  
259 cultivar using the wavelengths selected in the previous study for ripeness assessment.  
260 For each fruit there was obtained only one global value of the flesh firmness so the  
261 prediction model was built using the average values of the pixels selected for each fruit  
262 at the determined wavelengths of the hyperspectral images. Cross validation leaving 5%  
263 of samples for test was chosen to validate this study. This method splits randomly the  
264 data set into the training (95%) and test (5%), repeating the process 20 times. Results  
265 were achieved as the mean of the 20 repetitions.

266 The coefficient of determination for the prediction ( $R^2_P$ ) was 0.80 and the RPD was 1.86  
267  $\pm$  0.26. Viscarra-Rossel et al., (2006) suggested that calibration models will suffice for  
268 good quantitative application if RPD is larger than 1.8. The prediction results obtained  
269 was something higher than the minimum proposed but not as good as the prediction  
270 results of Wei et al., (2014) for 'Fangshi' persimmon who achieved a  $R^2$  value of 0.91.  
271 However, in their work the firmness of the fruit ranged from 25 N to 1 N with large  
272 differences among the studied classes. In addition, during the ripening process of this  
273 cultivar not only drastic changes in firmness happened but also the skin begins to  
274 wrinkle and lose shine clearly affecting the reflectance. On the contrary, in the present  
275 work, the firmness gave values from 47 N to 21 N which means that these fruits are  
276 apparently firm in all maturity stages, which is logical since it is treated to be consumed  
277 as firm and crispy fruit. Figure 1 highlights the visual differences between a soft  
278 persimmon naturally destringed and another destringed a using CO<sub>2</sub> treatment. Hence,  
279 for this fruit 80% of prediction capability is considered as a good achievement taking  
280 into account the little differences between classes, especially between M2 and M3  
281 classes.

282 A study was also carried out to analyse the possible correlation between the colour  
283 analysis and the firmness of the samples. The characterisation of the external colour was  
284 carried out using the colorimeter and the camera only for the control samples of the  
285 three stages to avoid the influence of the treatment in colour changes (Table 3). In  
286 general, the  $L$  and  $b$ , Hunter Lab coordinates, decreased but there were not statistical  
287 differences for M2 and M3. On the contrary, the value of  $a$  increased along the three  
288 stages. As a consequence of the changes observed in  $a$  and  $b$ , the hue decreased and the  
289 chroma slightly increased along the three stages. These differences were observed in the  
290 measures given by both, the colorimeter and the camera, and reflect the loss of  
291 luminosity of the fruit caused by the maturity process and the changes in the fruit from  
292 yellowish-orange to reddish-orange.

293 The values of the colour attributes ( $L$ ,  $h$  and  $C$ ) of the colorimeter were higher than the  
294 ones obtained from the images. The higher differences were observed for the  $L$  values  
295 since the glossiness leads to a specular reflectance that reduces the contribution to the  
296 components  $a$  and  $b$ . In fact, colorimeter is very dependent on the scattering properties  
297 of the sample while the diffuse illumination of the vision system gives less dependency  
298 on the lightness of the sample than the simple illumination and filtering employed by  
299 the colorimeter (Trinderup et al., 2015). Despite the differences observed, good  
300 correlations were found between the values obtained by both methods ( $R^2$  of 0.87,  
301 0.80, and 0.96 for the  $L$ , chroma, and hue respectively).

302 Linear regressions were performed between the different colour values, obtained with  
303 both the colorimeter and the camera, and the firmness. Table 4 and 5 summarise the  
304 results achieved for the coefficient of determination  $R^2$  for each colour component using  
305 the imaging system and the colorimeter, respectively. In general, better results are  
306 achieved with the imaging system which on the other hand makes sense since they

307 integrate the colour of the whole surface of the fruit while colorimeter only measures in  
308 a small spot and thus increasing the variability.

309 Good correlations are found in  $H$  ( $R^2=0.83$ ),  $G$  ( $R^2=0.82$ ) and  $h$  ( $R^2=0.81$ ) or using  
310 simple ratios like  $a/b$  ( $R^2=0.83$ ),  $G/R$  ( $R^2=0.83$ ) or  $a/L$  ( $R^2=0.83$ ). It is worthy of interest  
311 that using the simple ratios measured with the imaging system could be obtained better  
312 correlations ( $R^2=0.83$ ) than using the  $CI$  ( $CI=1000a/Lb$ ) that was the index used by  
313 Salvador et al., (2006) to estimate the firmness trough a colorimeter achieving a  
314  $R^2=0.81$ .

### 315 **3.1. Astringency prediction**

316 The results of the measurements of soluble tannins of fresh weight for all maturity  
317 stages are shown in Table 6. It can be observed that the tannin content decreased in a  
318 similar way for the three maturity stages along with the duration of the treatment. The  
319 soluble tannins content decreased to values close to 0.4% in the fruits treated for 12 h to  
320 0.03% in the fruits exposed for 24 h to  $CO_2$ . Accordingly, Besada et al., (2010) reported  
321 that the  $CO_2$ -treatment applied for 12 h to fruit with firmness around 40 N led to a  
322 reduction of soluble tannins to values close 0.3%. Besides, it has been widely reported  
323 that a content of soluble tannins of 0.03% after the  $CO_2$ -treatment is associated with a  
324 complete effectiveness of the deastringency process in ‘Rojo Brillante’ cultivar  
325 (Salvador et al., 2007; Salvador et al., 2008).

326 Like in ripeness classification, three PCA models were analysed to identify the highest  
327 factor loadings in each ripeness stage. However, no wavelength selection could  
328 contribute to the astringency classification. This may be because tannins are mainly  
329 detected in the ultraviolet (UV) in the range 190 to 400 nm (Boulet et al., 2016), or in  
330 the NIR (2200 to 2300 nm) (Cozzolino et al., 2004). For this reason, the whole spectrum  
331 in the studied range (450-1020 nm) was necessary to discriminate the astringency.

332 Table 7 shows the results of astringency classification using the three classifiers. In  
333 general, QDA obtained the best overall classification but a reduction of the  
334 classification rate along with the maturity was observed, especially for the astringent  
335 fruits (HA and LA) in the M3 stage. As it was shown in Table 2, a decrease of firmness  
336 in M1 between control and non astringent fruits was observed. However, in M2 and M3  
337 there was no difference. This could be due because the effect of high CO<sub>2</sub>  
338 concentrations on the cell structure could be the cause of the important loss of firmness  
339 observed after deastringency treatment. But when the more ripe samples are treated with  
340 CO<sub>2</sub>, no effect happens on flesh firmness because the loss of intercellular adhesion is  
341 already generalised due to the ripeness process (Salvador et al., 2007). Therefore, those  
342 changes detected by hyperspectral imaging are assigned to changes in the soluble  
343 tannins content and not to changes in texture.

#### 344 **4. Conclusions**

345 In this study, VIS/NIR hyperspectral imaging were evaluated as potential non-  
346 destructive methods to determine the flesh firmness, maturity stage and the astringency  
347 level of 'Rojo Brillante' persimmon.

348 The characterisation of the colour showed that the *L* and *b*, Hunter Lab coordinates  
349 decreased while the value of *a* increased along with the maturity. As a consequence the  
350 hue decreased and the chroma slightly increased along the three stages using both  
351 colorimeter and image methods. Good correlations were found in some colour  
352 parameters like *H* ( $R^2=0.83$ ), *G* ( $R^2=0.82$ ) and *h* ( $R^2=0.81$ ), but also using ratios like *a/b*  
353 ( $R^2=0.83$ ), *G/R* ( $R^2=0.83$ ) and *a/L* ( $R^2=0.83$ ) with the data obtained by the imaging  
354 system improving previous results. Moreover, better correlations were obtained using  
355 these ratios than using the previously proposed CI ( $R^2=0.80$ ) which indicates the

356 feasibility of images to assess the colour as a valid alternative to traditional and  
357 expensive colorimeters.

358 Using the hyperspectral system, three wavelengths (580, 680 and 1050 nm) were  
359 proposed as the optimum wavelengths for the classification of the fruits into three  
360 ripeness stages with high accuracy, more than 94% of all samples were well classified  
361 for all of the used classifiers (LDA, QDA and SVM). Moreover, these wavelengths  
362 were used for flesh firmness prediction and the RPD value indicated that the obtained  
363 model is useful for good quantitative application. Regarding the astringency, the whole  
364 spectrum of the fruits needed to be used to classify the fruits into three levels of  
365 astringency: astringent fruit, fruit with a low-medium level of astringency and non-  
366 astringent fruit. The overall classification for the three ripeness stages was higher than  
367 90% for the three classifiers and higher than 95% for QDA. These results indicate the  
368 potential proposed methodology based on hyperspectral imaging as a promising non-  
369 destructive tool to assess the internal quality of persimmon fruits destined to be  
370 deastringed and rapidly marketed as fresh sweet fruit. However, more research is  
371 needed, involving more fruits from different regions and collected in different seasons  
372 to ascertain the discrimination power of the proposed methodology in other markets and  
373 conditions.

#### 374 **Acknowledgements**

375 This work has been partially funded by the INIA through projects RTA2012-00062-  
376 C04-01, RTA2012-00062-C04-03 and RTA2013-00043-C02 with FEDER funds, GVA  
377 through the project AICO/2015/122, and the International S&T Cooperation Programs  
378 of China (2015DFA71150) and Guangdong Province, China (2013B051000010).  
379 Sandra Munera thanks INIA for the grant FPI-INIA #43 (CPR2014-0082) partially  
380 supported by FSE funds.

381

#### 382 **References**

383 Arnal, L., del Río, M.A. (2004). Quality of persimmon fruit cv. 'Rojo Brillante' during  
384 storage at different temperatures. Spanish Journal of Agricultural Research, 2, 243–  
385 247.

386 Besada, C., Salvador, A., Arnal, L., Martínez-Jávega, J.M. (2010). Optimization of the  
387 duration of destringency treatment depending on persimmon maturity. *Acta*  
388 *Horticulturae*, 858, 69–74.

389 Cheng, J.H. Sun, D.-W. (2015). Rapid and non-invasive detection of fish microbial  
390 spoilage by visible and near infrared hyperspectral imaging and multivariate analysis.  
391 *LWT - Food Science and Technology*, 62, 1060-1068.

392 Cheng, W., Sun, D.-W., Cheng, J.H. (2016). Pork biogenic amine index (BAI)  
393 determination based on chemometric analysis of hyperspectral imaging data. *LWT -*  
394 *Food Science and Technology*, 73, 13-19.

395 Cheng, W., Sun, D.-W., Pu, H., Liu, Y. (2016). Integration of spectral and textural data  
396 for enhancing hyperspectral prediction of K value in pork meat. *LWT - Food Science*  
397 *and Technology*, 72, 322-329.

398 Cozzolino, D., Kwiatkowski, M.J., Parker, M., Cynkar, W.U., Damberg, R.G., Gishen,  
399 M., Herderich, M.J. (2004). Prediction of phenolic compounds in red wine  
400 fermentations by visible and near infrared spectroscopy. *Analytica Chimica Acta*,  
401 513, 73–80.

402 Diago, M.P., Tardaguila, J., Aleixos, N., Millan, B., Prats-Montalban, J.M., Cubero, S.,  
403 Blasco, J. (2015). Assessment of cluster yield components by image analysis. *Journal*  
404 *of the Science of Food and Agriculture*, 95, 1274-1282.

405 Dutta, M.K., Sengar, N., Minhas, N., Sarkar, B., Goon, A., Banerjee K. (2016). Image  
406 processing based classification of grapes after pesticide exposure. *LWT - Food*  
407 *Science and Technology*, 72, 368-376.

408 ElMasry, G., Cubero, S., Moltó, E., Blasco, J. (2012). In-line sorting of irregular  
409 potatoes by using automated computer-based machine vision system. *Journal of Food*  
410 *Engineering*, 112, 60-68.

411 ElMasry, G., Wang, N., Vigneault, C., Qiao, J., ElSayed A. (2008). Early detection of  
412 apple bruises on different background colors using hyperspectral imaging. *LWT -*  
413 *Food Science and Technology*, 41, 337-345.

414 Folch-Fortuny, A., Prats-Montalbán, J.M., Cubero, S., Blasco, J., Ferrer, A. (2016). NIR  
415 hyperspectral imaging and N-way PLS-DA models for detection of decay lesions in  
416 citrus fruits. *Chemometrics and Intelligent Laboratory Systems*, 156, 241-248.

417 Gat, N. (2000). Imaging spectroscopy using tunable filters: A review. Technical report,  
418 Opto-Knowledge Systems Inc. OKSI.



419 Gómez-Sanchis, J., Blasco, J., Soria-Olivas, E., Lorente, D., Escandell-Montero, P.,  
420 Martínez-Martínez, J.M., Martínez-Sober, M., Aleixos, N. (2013). Hyperspectral  
421 LCTF-based system for classification of decay in mandarins caused by *Penicillium*  
422 *digitatum* and *Penicillium italicum* using the most relevant bands and non-linear  
423 classifiers. *Postharvest Biology and Technology*, 82, 76-86.

424 HunterLab. (1996). Applications note, Hunter Lab Color Scale.  
425 [https://support.hunterlab.com/hc/en-](https://support.hunterlab.com/hc/en-us/article_attachments/201440625/an08_96a2.pdf)  
426 [us/article\\_attachments/201440625/an08\\_96a2.pdf](https://support.hunterlab.com/hc/en-us/article_attachments/201440625/an08_96a2.pdf), Accessed November 2016.

427 Hutchings, J.B., (1999). Food color appearance. In: *Food Color Mechanisms*, pp. 453–  
428 592. Aspen Publishers, Inc, Gaithersburg, Maryland (USA).

429 Lorente D., Aleixos, N., Gómez-Sanchis, J., Cubero, S., García-Navarrete, O.L., Blasco,  
430 J. (2012). Recent advances and applications of hyperspectral imaging for fruit and  
431 vegetable quality assessment. *Food and Bioprocess Technology*, 5, 1121–1142.

432 Lu, R., Peng, Y. (2006). Hyperspectral Imaging for assessing peach fruit firmness.  
433 *Biosystems Engineering*, 93, 161–171.

434 Matsuo, T., Ito, S., Ben-Arie, R. (1991). A model experiment for elucidating the  
435 mechanism of astringency removal in persimmon fruit using respiration inhibitors.  
436 *Journal of the Japanese Society for Horticultural Science*, 60, 437–442.

437 Mendoza, F., Dejmek, P., Aguilera, J.M. (2006). Calibrated color measurements of  
438 agricultural foods using image analysis. *Postharvest Biology and Technology*, 41, 285-  
439 295.

440 Mohammadi, V., Kheiralipour, K., Ghasemi-Varnamkhasti, M. (2015). Detecting  
441 maturity of persimmon fruit based on image processing technique. *Scientia*  
442 *Horticulturae*, 184, 123–128.

443 Munera, S., Besada, C., Blasco, J., Cubero, S., Salvador, A., Talens, P., Aleixos, N.  
444 (2016). Astringency assessment of persimmon by hyperspectral imaging. *Postharvest*  
445 *Biology and Technology*, 125, 35-41.

446 Naes, T., Isaksson, T., Fearn, T., Davies, T. (2002). *A User-friendly Guide to*  
447 *Multivariate Calibration and Classification*. NIR Publications, Chichester.

448 Plaza, L., Colina, C., de Ancos, B., Sanchez-Moreno, C., Cano, M.P. (2012). Influence  
449 of ripening and astringency on carotenoid content of high-pressure treated  
450 persimmon fruit (*Diospyros kaki* L.). *Food Chemistry*, 130, 591–597

451 Rodríguez-Pulido F.J., Barbin, D.F., Sun, D.-W., Gordillo, B., González-Miret M.L.,  
452 Heredia, F.J. (2013). Grape seed characterization by NIR hyperspectral imaging.  
453 *Postharvest Biology and Technology*, 76, 74–82.

454 Salvador, A., Arnal, L., Besada, C., Larrea, V., Quiles, A., Pérez-Munuera, I. (2007).  
455 Physiological and structural changes during ripening and destringency treatment of  
456 persimmon cv. ‘Rojo Brillante’. *Postharvest Biology and Technology*, 46, 181–188.

457 Salvador, A., Arnal, L., Besada, C., Larrea, V., Hernando, I., Pérez-Munuera, I. (2008).  
458 Reduced effectiveness of the treatment for removing astringency in persimmon fruit  
459 when stored at 15 °C: Physiological and microstructural study. *Postharvest Biology*  
460 *and Technology*, 49, 340–347.

461 Salvador, A., Arnal, L., Carot, J.M., Carvalho, C., Jabaloyes, J.M. (2006). Influence of  
462 different factors on firmness and color evolution during the storage of persimmon cv.  
463 ‘Rojo Brillante’. *Journal of Food Science*, 71, 169–175.

464 Schmilovitch, Z., Ignat, T., Alchanatis, V., Gatker, J., Ostrovsky, V., Felföldi, J. (2014).  
465 Hyperspectral imaging of intact bell peppers. *Biosystems Engineering*, 117, 83-93.

466 Simon, R. (2007) Resampling strategies for Model Assessment and selection chapter 8,  
467 pp.173-186 in *Fundamentals of Data Mining in Genomics and Proteomics* Dubitzky,  
468 Granzow and Berra reds). Springer, NY USA

469 Taira, S. (1995). ‘Astringency in persimmon’. In: Linskens, H.F., Jackson, J.F. *Fruit*  
470 *Analysis*. Springer, Hannover, Germany, pp. 97–110.

471 Trinderup, C.H., Dahl, A., Jensen, K., Carstensen, J.M., Conradsen, K. (2015).  
472 Comparison of a multispectral vision system and a colorimeter for the assessment of  
473 meat color. *Meat Science*, 102, 1–7.

474 Vélez-Rivera, N., Gómez-Sanchis, J., Chanona-Pérez, J.J., Carrasco, J.J., Millán-  
475 Giraldo, M., Lorente, D., Cubero, S., Blasco, J. (2014). Early detection of  
476 mechanical damage in mango using NIR hyperspectral images and machine learning.  
477 *Biosystems Engineering*, 122, 91-98.

478 Viscarra-Rossel, A., McGlynn, R.N., McBratney, A.B. (2006). Determining the  
479 composition of mineral-organic mixes using UV–vis–NIR diffuse reflectance  
480 spectroscopy. *Geoderma*, 137, 70–82.

481 Wang, W., Li, C., Tollner, E.W., Gitaitis, R.D., Rains G.C. (2012). Shortwave infrared  
482 hyperspectral imaging for detecting sour skin (*Burkholderia cepacia*)-infected  
483 onions. *Journal of Food Engineering*, 109, 38–48.

- 484 Wei, X., Liu, F., Qiu, Z., Shao, Y., He, Y. (2014). Ripeness classification of astringent  
485 persimmon using hyperspectral imaging technique. *Food and Bioprocess*  
486 *Technology*, 7, 1371–1380.
- 487 Williams, P.C. (1987). Variables affecting near-infrared reflectance spectroscopic  
488 analysis. In: Williams, P., Norris, K. *Near-infrared Technology in the Agricultural*  
489 *and Food Industries*. American Association of Cereal Chemists, St. Paul, MN, pp.  
490 143–166.

491  
492  
493  
494  
495

Tables

Table 1. Ripeness classification of testing set by LDA, QDA and SVM using all and selected wavelengths (cross validation)

Class	All wavelengths			Selected wavelengths		
	LDA	QDA	SVM	LDA	QDA	SVM
M1	99.5 ± 0.8 <sup>a</sup>	99.8 ± 0.4 <sup>a</sup>	99.1 ± 1.0 <sup>a</sup>	98.6 ± 0.0 <sup>a</sup>	99.3 ± 0.7 <sup>a</sup>	98.4 ± 0.4 <sup>a</sup>
M2	96.8 ± 3.2 <sup>a</sup>	96.2 ± 2.9 <sup>a</sup>	96.0 ± 2.7 <sup>a</sup>	95.5 ± 2.5 <sup>a</sup>	94.1 ± 2.2 <sup>a</sup>	94.7 ± 2.6 <sup>a</sup>
M3	99.0 ± 0.8 <sup>a</sup>	100 ± 0.0 <sup>a</sup>	99.8 ± 0.4 <sup>a</sup>	83.7 ± 2.3 <sup>a</sup>	93.9 ± 2.9 <sup>b</sup>	94.9 ± 1.5 <sup>b</sup>
<i>Total</i>	98.5 ± 2.1 <sup>a</sup>	98.8 ± 2.2 <sup>a</sup>	98.3 ± 2.3 <sup>a</sup>	92.6 ± 7.1 <sup>a</sup>	95.8 ± 3.3 <sup>a</sup>	96.0 ± 2.4 <sup>a</sup>

496 *Values are the mean of three models ± standard deviation. Different superscript letters in the same row*  
497 *indicate significant differences between groups (p-value<0.05), according to Tukey's test.*

498  
499

Table 2. Flesh firmness (in N) of ‘Rojo Brillante’ persimmon fruits before and after treatments in the three ripeness stages

Group	M1	M2	M3
HA	47.0 <sup>a</sup> ± 4.3 <sub>a</sub>	29.0 <sup>a</sup> ± 2.6 <sub>b</sub>	25.1 <sup>a</sup> ± 3.4 <sub>c</sub>
LA	44.7 <sup>ab</sup> ± 2.6 <sub>a</sub>	30.9 <sup>a</sup> ± 3.0 <sub>b</sub>	25.0 <sup>a</sup> ± 4.7 <sub>c</sub>
NA	40.6 <sup>b</sup> ± 2.8 <sub>a</sub>	31.9 <sup>a</sup> ± 2.1 <sub>b</sub>	21.1 <sup>a</sup> ± 4.8 <sub>c</sub>

502 *Values are the flesh firmness (N) ± standard deviation. Different superscript letters in the same column*  
503 *(astringency) and different subscript letters in the same row (ripening) indicate significant differences*  
504 *between groups (p-value<0.05), according to Tukey's test.*

505  
506

Table 3. Colour coordinates and attributes of the samples in the three harvests

Stage	Colorimeter					Imaging				
	L	a	b	h	C	L	a	b	h	C
M1	58.93 ±1.83 <sup>a</sup>	21.71 ±3.29 <sup>c</sup>	34.84 ±1.75 <sup>a</sup>	60.29 ±4.41 <sup>a</sup>	40.67 ±1.61 <sup>c</sup>	43.75 ±1.03 <sup>a</sup>	27.82 ±3.54 <sup>c</sup>	26.03 ±0.53 <sup>a</sup>	49.51 ±4.42 <sup>a</sup>	36.32 ±2.00 <sup>c</sup>
M2	53.49 ±1.94 <sup>b</sup>	34.49 ±1.80 <sup>b</sup>	31.20 ±1.41 <sup>b</sup>	46.46 ±4.60 <sup>b</sup>	45.42 ±1.64 <sup>b</sup>	33.88 ±2.44 <sup>b</sup>	38.30 ±2.54 <sup>b</sup>	20.51 ±1.35 <sup>b</sup>	34.46 ±3.78 <sup>b</sup>	42.07 ±1.64 <sup>b</sup>
M3	52.64 ±1.38 <sup>b</sup>	38.38 ±1.65 <sup>a</sup>	30.77 ±1.09 <sup>b</sup>	39.20 ±1.90 <sup>c</sup>	48.29 ±0.53 <sup>a</sup>	34.71 ±1.95 <sup>b</sup>	41.24 ±1.40 <sup>a</sup>	21.02 ±1.05 <sup>b</sup>	28.62 ±1.78 <sup>c</sup>	43.64 ±1.26 <sup>a</sup>

508 *Values are the mean of control samples in each harvest ± standard deviation. Different superscript letters*  
509 *in the same column indicate significant differences between groups (p-value<0.05), according to Tukey's*  
510 *test.*

511

512  
513

Table 4. Coefficient of determination for the firmness and the different colour components measured with the imaging system

	<i>R</i>	<i>G</i>	<i>B</i>	<i>H</i>	<i>S</i>	<i>I</i>	<i>G/R</i>
$R^2$	0.49	0.82	0.46	0.83	0.48	0.17	0.83

	<i>L</i>	<i>a</i>	<i>b</i>	<i>CI</i>	<i>a/b</i>	<i>a/L</i>	<i>h</i>	<i>C</i>
$R^2$	0.79	0.78	0.78	0.80	0.83	0.83	0.81	0.69

514  
515  
516  
517  
518  
519  
520

*R* red, *G* green, *B* blue, *H* hue, *S* saturation, *I* intensity, *L* Hunter luminosity, *a* Hunter *a* value, *b* Hunter *b* value, *CI* colour index, *h* Hunter hue, *C* Hunter chroma

521  
522

Table 5. Coefficient of determination for the firmness and the different colour components measured with the colorimeter

	<i>L</i>	<i>a</i>	<i>b</i>	<i>CI</i>	<i>a/b</i>	<i>a/L</i>	<i>h</i>	<i>C</i>
$R^2$	0.66	0.78	0.63	0.77	0.78	0.78	0.77	0.76

523  
524  
525  
526  
527  
528  
529

*L* Hunter luminosity, *a* Hunter *a* value, *b* Hunter *b* value, *CI* colour index, *h* Hunter hue, *C* Hunter chroma

530  
531

Table 6. Soluble tannins content (%) in ‘Rojo Brillante’ persimmon fruits before and after treatments in the three ripeness stages

Group	M1	M2	M3
HA	0.61 <sup>a</sup> ± 0.09	0.65 <sup>a</sup> ± 0.06	0.63 <sup>a</sup> ± 0.07
LA	0.45 <sup>b</sup> ± 0.04	0.43 <sup>b</sup> ± 0.10	0.39 <sup>b</sup> ± 0.06
NA	0.03 <sup>c</sup> ± 0.00	0.03 <sup>c</sup> ± 0.00	0.03 <sup>c</sup> ± 0.00

532  
533  
534  
535  
536

Values are the mean of three measures of soluble tannins content (%) ± standard deviation. Different superscript letters in the same column indicate significant differences between groups (*p*-value < 0.05), according to Tukey's test.

537

538

Table 7. Astringency classification of test set by LDA, QDA and SVM

Class	Correct classification (%)			
	LDA	QDA	SVM	
M1	HA	95.9 ± 0.0 <sup>b</sup>	99.3 ± 0.0 <sup>a</sup>	97.1 ± 0.8 <sup>b</sup>
	LA	92.4 ± 4.0 <sup>a</sup>	94.5 ± 4.3 <sup>a</sup>	94.9 ± 2.2 <sup>a</sup>
	NA	93.9 ± 2.6 <sup>a</sup>	97.3 ± 1.5 <sup>a</sup>	93.2 ± 2.1 <sup>a</sup>
	Avg	94.1 ± 2.8 <sup>a</sup>	97.0 ± 3.1 <sup>a</sup>	95.1 ± 2.3 <sup>a</sup>
M2	HA	93.2 ± 2.5 <sup>a</sup>	96.2 ± 2.1 <sup>a</sup>	92.7 ± 1.7 <sup>a</sup>
	LA	93.0 ± 3.4 <sup>a</sup>	95.3 ± 2.2 <sup>a</sup>	91.1 ± 3.9 <sup>a</sup>
	NA	93.9 ± 1.1 <sup>a</sup>	95.6 ± 2.6 <sup>a</sup>	95.9 ± 1.5 <sup>a</sup>
	Avg	93.4 ± 2.2 <sup>a</sup>	95.7 ± 2.1 <sup>a</sup>	93.2 ± 3.1 <sup>a</sup>
M3	HA	83.7 ± 0.7 <sup>b</sup>	94.3 ± 1.6 <sup>a</sup>	90.0 ± 3.4 <sup>a</sup>
	LA	72.0 ± 3.4 <sup>b</sup>	86.0 ± 3.4 <sup>a</sup>	64.5 ± 2.2 <sup>b</sup>
	NA	93.4 ± 2.2 <sup>a</sup>	97.3 ± 1.5 <sup>a</sup>	93.4 ± 0.7 <sup>a</sup>
	Avg	83.0 ± 9.5 <sup>a</sup>	92.5 ± 5.5 <sup>a</sup>	82.7 ± 13.8 <sup>a</sup>
Overall classification (%)	90.2 ± 7.6 <sup>b</sup>	95.1 ± 4.1 <sup>a</sup>	90.3 ± 9.7 <sup>b</sup>	

539

Values are the mean of three models ± standard deviation. Different superscript letters in the same row indicate significant differences between groups ( $p$ -value < 0.05), according to Tukey's test.

540

541

542

543

544 Captions of the figures

545

546

547 Figure 1. Persimmon destringed using a CO<sub>2</sub> treatment (left) and persimmon naturally

548 destringed by overripeness (right). The first shows firm and crisp flesh while the

549 second present a very soft texture.

550

551 Figure 2. Images of persimmon at maturity stage M1, M2 and M3 from left to right.

552

553 Figure 3. Hyperspectral acquisition system

554

555 Figure 4. Images of a persimmon (M1) with selected ROI: (a) colour image;

556 hyperspectral image with (b) the VIS filter centred in 640 nm; and with (c) the NIR

557 filter centred in 900 nm

558

559 Figure 5. Average spectra of control fruits in three ripeness stages M1 (long dashed

560 line), M2 (medium dashed line) and M3 (short dashed line)

561

562 Figure 6. PC Loadings of the PC1 (solid line) and PC2 (dashed line) showing the

563 selected wavelengths for ripeness classification of 'Rojo Brillante' persimmon fruits.

564

565

566

567

Figure  
[Click here to download high resolution image](#)





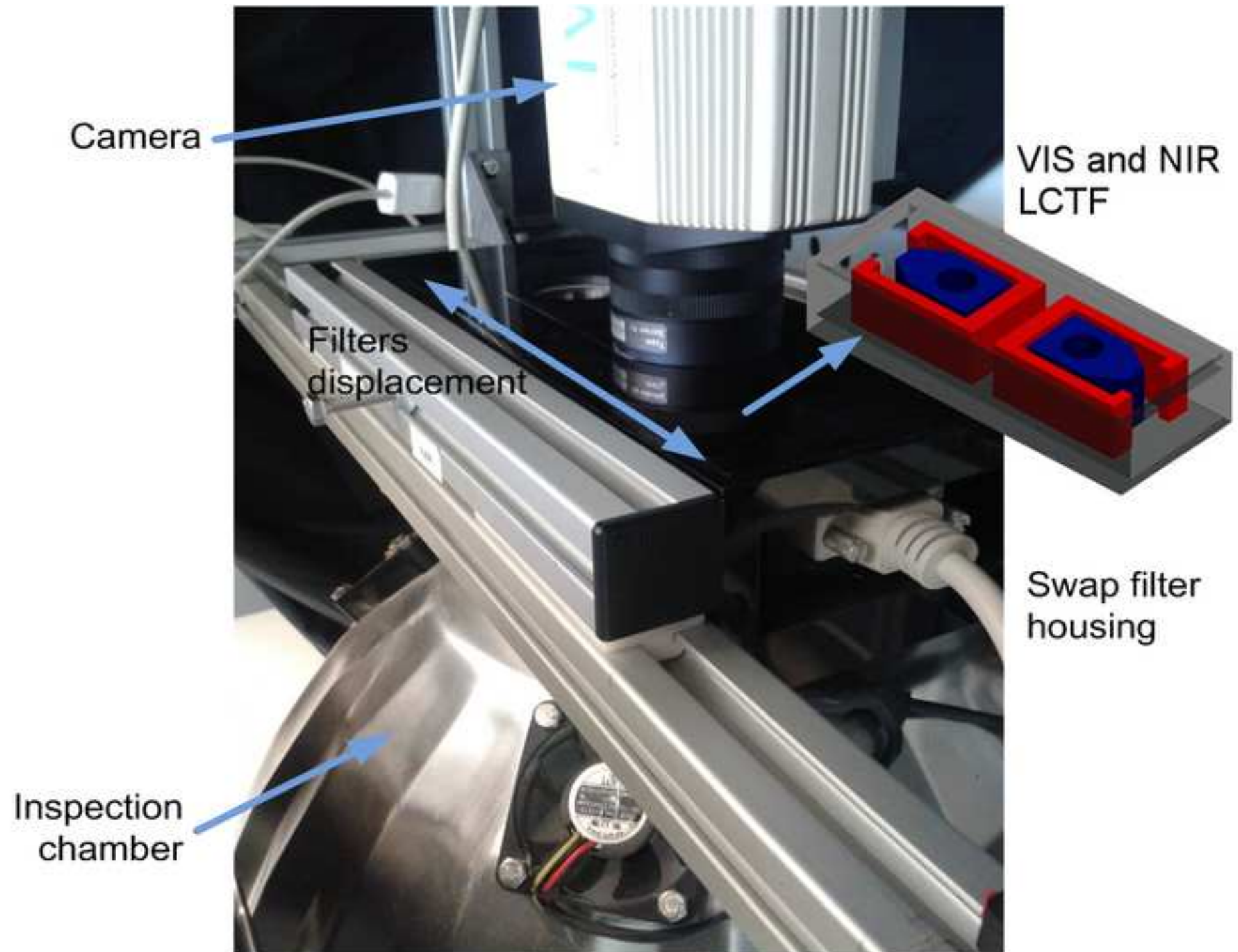
Figure

[Click here to download high resolution image](#)



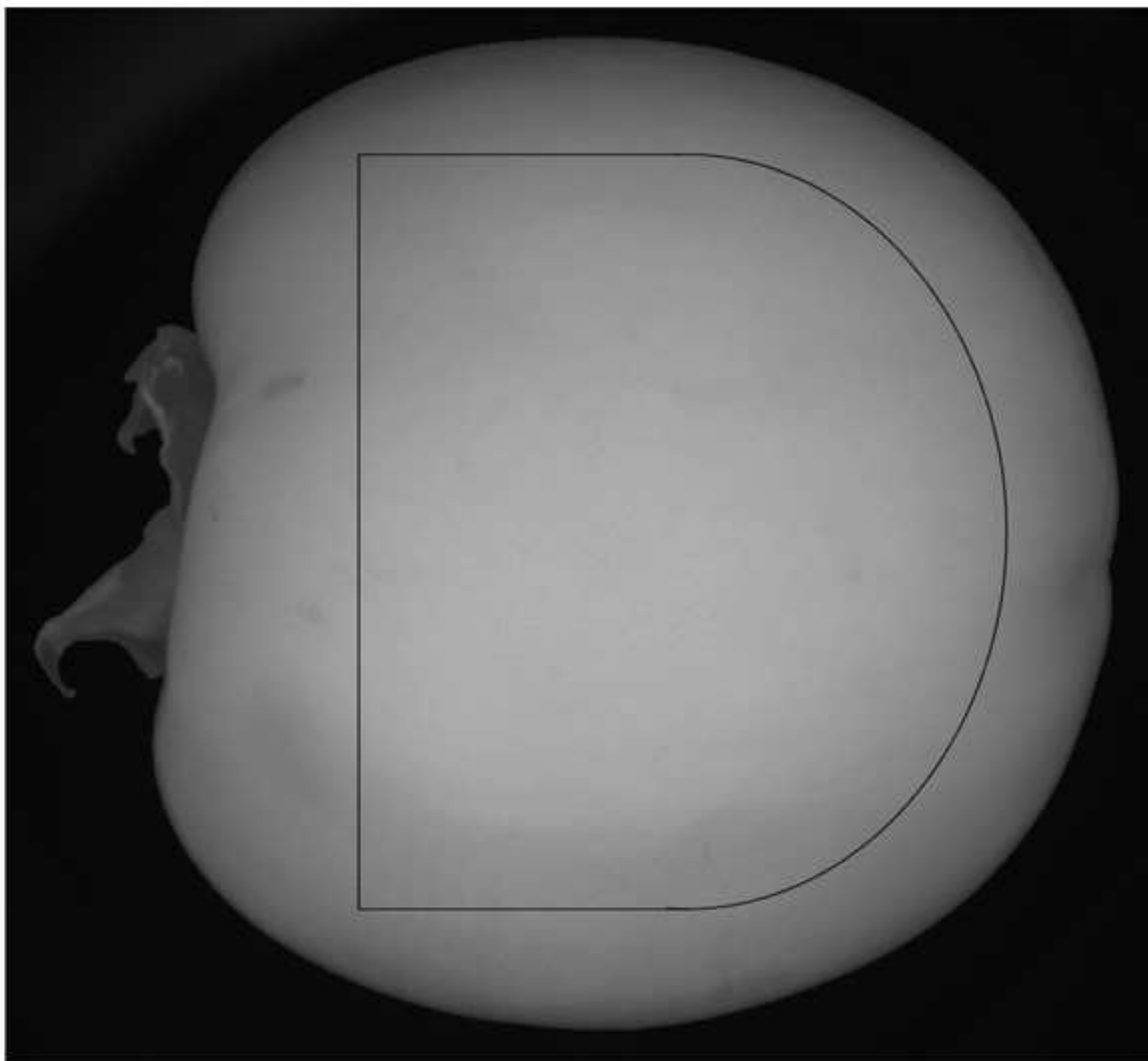
Figure

[Click here to download high resolution image](#)



Figure

[Click here to download high resolution image](#)



Figure

[Click here to download high resolution image](#)

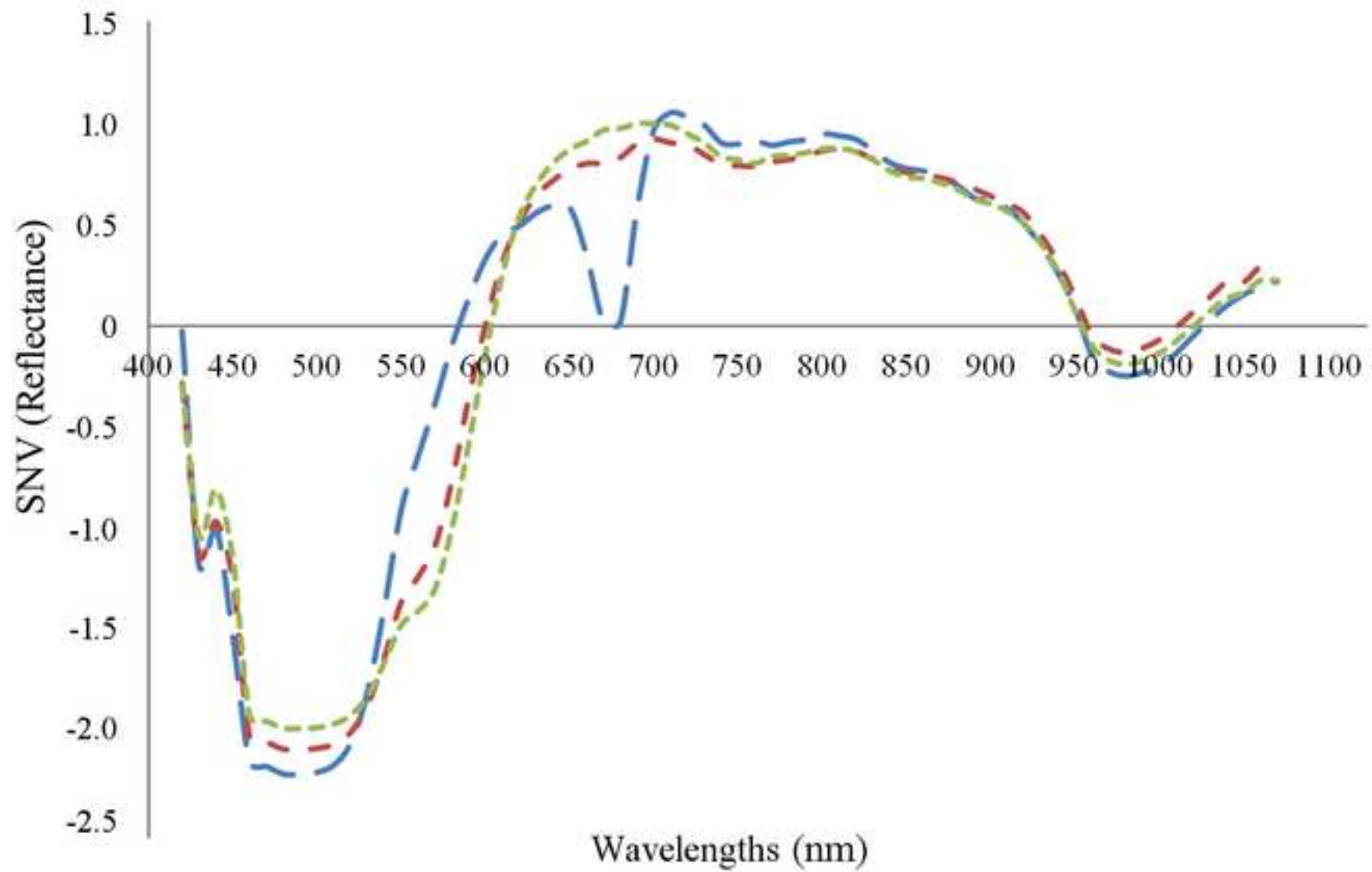


Figure  
[Click here to download high resolution image](#)

